Electronic Supplementary Material (ESI) for Journal of Materials Chemistry A.

Twist Angle Can Expand Charge Carrier Diffusion Length in Bilayer Black Phosphorus: Ab Initio Quantum Dynamics

Yonghao Zhu[1], Run Long[1*]

[1]College of Chemistry, Key Laboratory of Theoretical & Computational Photochemistry of Ministry of Education, Beijing Normal University, Beijing, 100875, P. R. China

1. Simulation Details

Our calculations are carried out using the Vienna ab initio Simulation Package (VASP)[1] and Quickstep/CP2K package.[2] The former is used for geometry optimization, electronic structure calculations, and carrier mobility, and the latter is applied to perform MD and NA couplings (NACs) calculations. In all calculations, the Perdew-Burke-Ernzerhof (PBE)[3] exchange-correlation functional is adopted. Van der Waals (vdW) interactions are described by Grimme DFT-D3 method,[4] and verified by optB88-vdW functional.[5-6] For the VASP calculations, the projector-augmented wave (PAW) is adopted to describe electron-ion core interaction,[7] and the plane-wave energy cutoff is set to 400 eV.[8-9] While the DZVP-MOLOPT-SR-GTH basis sets and Goedecker-Teter-Hutter (GTH) pseudopotentials are used in the Quickstep/CP2K simulations.[10-11] The mixed Gaussian and plane wave basis set with a cutoff of 400 Ry is employed to converge the total energy. Then, MD simulation is used to generate 8 ps trajectories in the canonical ensemble with a 1 fs atomic time step at the Γ point because all the three systems have a direct bandgap at the Γ point. The last 2000 geometries were chosen from equilibrated trajectory to calculate NACs at the Γ point by using nano-qmflows.[12] The phonon-assisted electron-hole recombination is simulated with the PYXAID code.[13-14] In order to reduce the computational cost of a long time NA-MD simulation, we perform short-time NA-MD simulation to get the transition rates between the CBM and VBM by fitting with the short-time linear approximation to the exponential function, $P(t) = exp(-t/\tau) \approx 1 - t/\tau$. Then, we solve the coupled kinetic equations using the obtained rates to obtain long-time NA-MD results shown in Figure 5.

---

[*] Corresponding author, E-mail: runlong@bnu.edu.cn

2. Interlayer Coupling

Interlayer coupling plays a key role to affect the properties in layered materials, especially in Moiré superlattice. In the multilayer BP including bulk system, the type of stacking is AB, and other stackings are not stable in terms of energies. However, the systems with twist angles contain four high-symmetry patterns (**Fig. 1c**), particularly in the small angles. The pervious works believe that the AA' and AB' stackings appear stronger interactions than AA and AB stackings, because of localization on transitional regions between two layers for CBM states (**Fig. 2e and S4**).[15-17] But interlayer distance of AB stacking is minimum (**Table S1**), which is dominant to the interlayer coupling generally,[18-19] in another word, the interactions in AB stacking are strongest than others, contributing to the type of stacking in multilayer BP. We demonstrate that the interactions are determined by interlayer distance (**Table S1**). **Fig. 2c and S3b** show the relationships between total energies and interlayer distance manually controlled, and the interaction energy of AB stacking is largest than other stackings, listed in **Table S1**. We note that the conclusions agree well with Shulenburger et al.[20] and Hu et al.[21] for bilayer BP systems.

4. Hole and Electron Effective Mass and Mobility

The deformation potential theory (DPT) proposed by Bardeen and Chockley[22] has been extensively applied to study mobility of 2D materials, such as multilayer BP,[23] InSe,[24] and transition-metal dichalcogenides (TMDs),[25] which are closed to experimental results. The carrier mobility is given by the following expression:

$$\mu_{2D} = \frac{e\hbar^3 C_{2D}}{k_B T m^* m_d E_1^2} \qquad \text{(S2)}$$

where m^* and $m_d = \sqrt{m_x^* m_y^*}$ are the effective mass along transport direction and average effective mass for different directions, respectively. E_1 is the deformation potential constant of the band edges, defined by $E_1 = \Delta V/(\Delta l/l_0)$. Here ΔV and l_0 are the energy change of band edges and lattice constant, respectively. Δl is the deformation of l_0. The elastic modulus C_{2D} can be calculated by $2[\partial^2 E_{tot}/\partial(\Delta l/l_0)^2]/S_0$, where E_{tot} is the total energy of system, and S_0 is the area of lattice. T is the temperature. e, $\hbar$, and k_B is the elementary charge, reduced Planck constant, and Boltzmann constant. When the units of effective mass (m^* and m_d), deformation potential (E_1), and elastic modulus (C_{2D}) are m_0(electronic rest mass), eV, and j/m^2, the equation can be written as:

$$\mu_{2D} = 21.3728 * \frac{1}{m^* m_d} * \frac{C_{2D}}{E_1^2} \qquad \text{(S3)}$$

The average mobility is calculated by $\frac{2}{\mu} = \frac{1}{\mu_Y} + \frac{1}{\mu_X}$, which is same to average effective mass of carrier.[26-27]

5. Kinetic Models

The VBM and CBM correspond to the ground (GS) and excited states (ES), respectively. The population growth of the ES is shown **Fig. S9**. Fits of the data in **Fig. S9** using the short-time linear approximation of the exponential functional, $P(t) = exp(- t/\tau) \approx 1 - t/\tau$, gives the transition rates between the CBM and VBM. The coupled kinetic equations for electron-hole recombination are as following:[28]

$$\frac{d[ES]}{dt} =- k[ES] \tag{S4}$$

$$\frac{d[GS]}{dt} = k[ES] \tag{S5}$$

where k, $[ES]$, and $[GS]$ are the rate constant, the population of ES and GS, respectively. The solutions of above equations are:

$$[ES] = e^{- kt} \tag{S6}$$

$$[GS] = 1 - e^{- kt} \tag{S7}$$

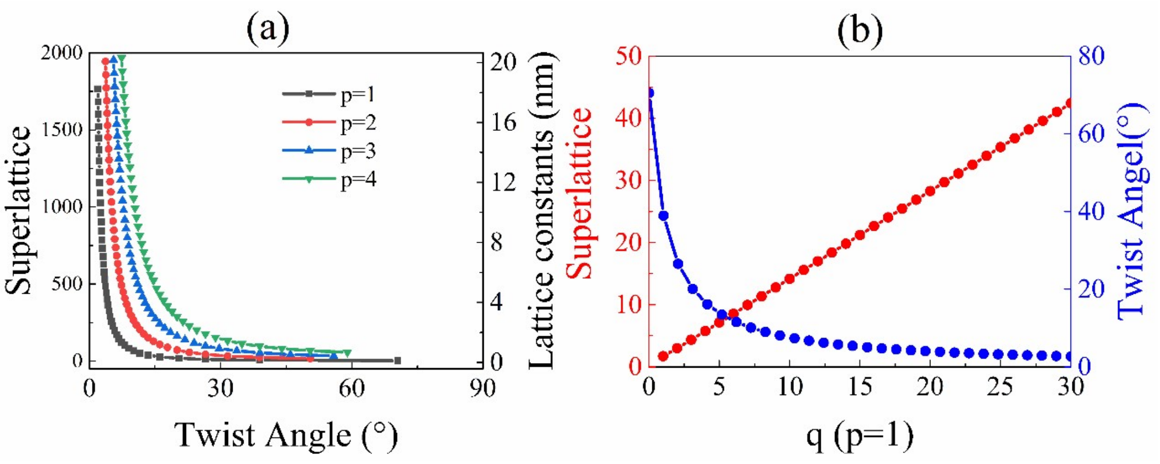

Figure S1. The relationship between superlattice and twist angle with (a) different *p* and *q* values and (b) *p*=1 for bilayer BP. The smaller twist angles are corresponding to the larger superlattice. We set *p*=1 to minimize the number of atoms of the bilayer BP systems under investigation.

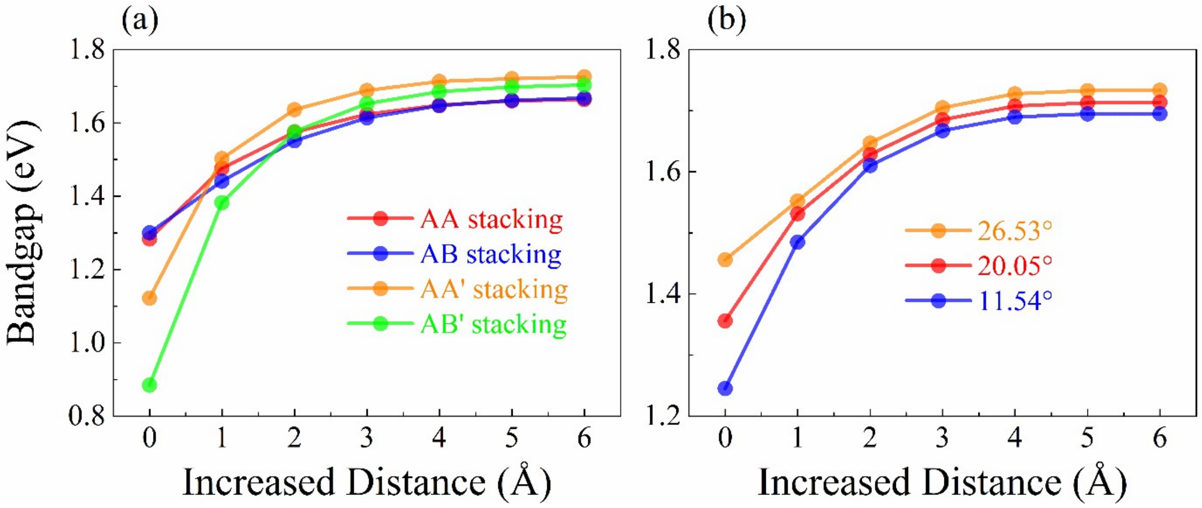

Figure S2. The interlayer distance dependent bandgaps in (a) high-symmetry stackings and (b) twisted systems calculated by DFT-D3[4]. With the increase of interlayer distance, the bandgaps gradually increase, which suggests decoupling between two layers. **Fig. 2c and 2d** show the interlayer distance dependent total energy difference. We indicate that there are no interactions in bilayer BP, when the increased distance equals 6 Å.

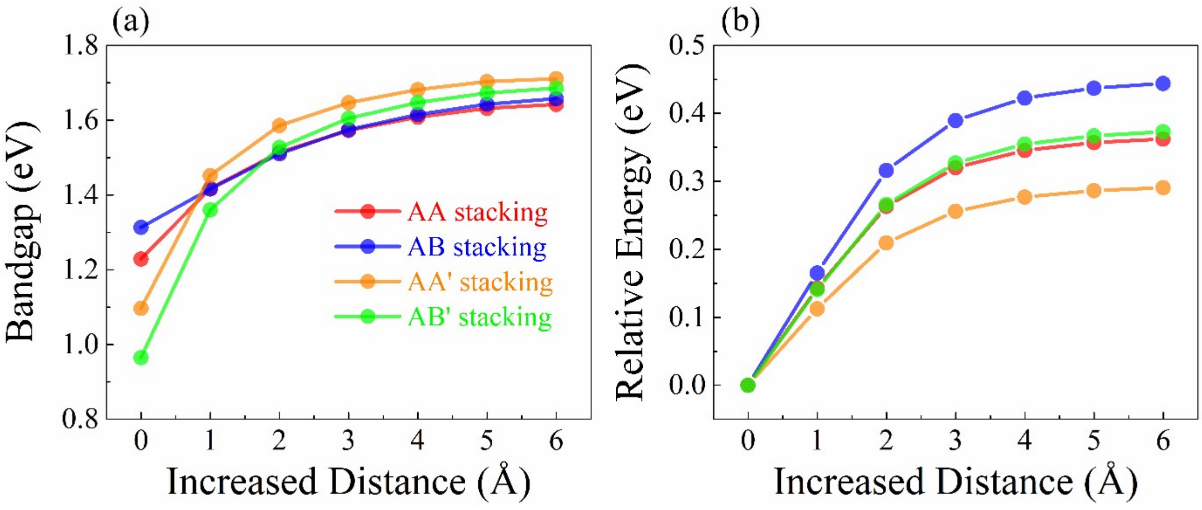

Figure S3. The interlayer distance dependent (a) bandgap and (b) total energy difference in high-symmetry stackings, including AA, AB, AA', and AB' stackings, which are calculated by optB88-vdW[5-6]. The variation tendencies of bandgaps and total energy difference justify the DFT-D3 method (**Fig. 2c and S2a**).[4]

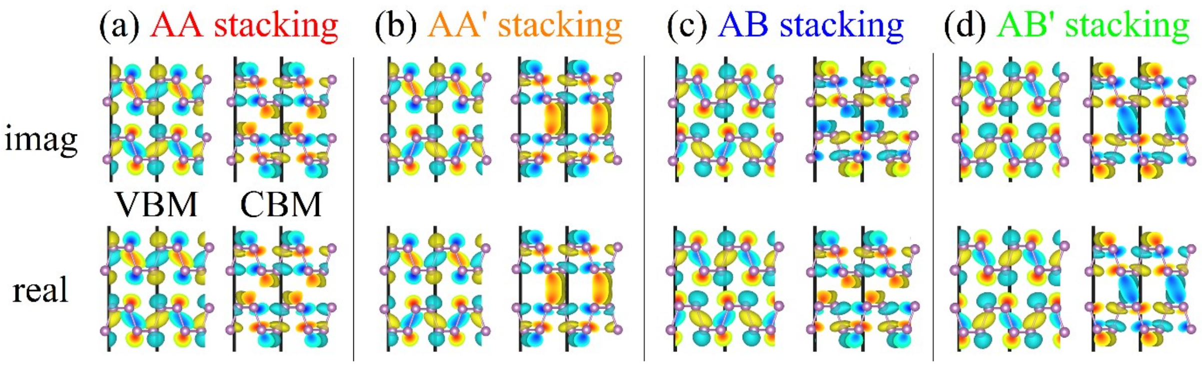

Figure S4. Imaginary (imag) and real component wavefunctions square of the VBM and CBM for the (a) AA, (b) AA’, (c) AB, and (d) AB’ staking configurations, calculated by optB88-vdW.[5-6] The results are identical with DFT-D3 method (**Fig. 2e**).[4]

Twist Angle (p q)	Superlattice	Interlayer Distance (Å)	VBM	CBM
70.53° (1 1)	3	3.08	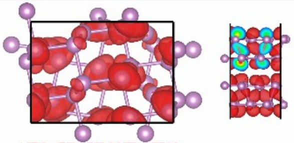	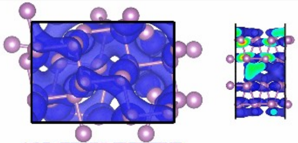
55.88° (3 4)	41	3.15	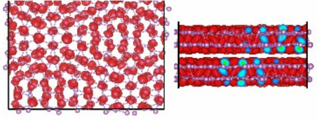	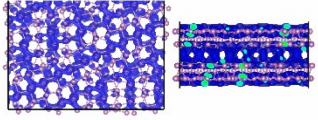
50.47° (2 3)	11	3.19	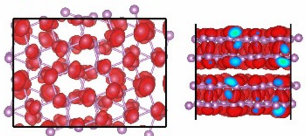	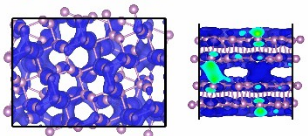
38.94° (1 2)	9	3.22	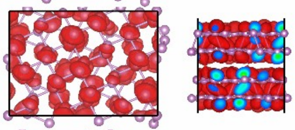	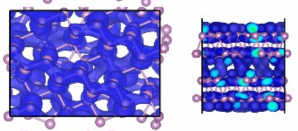
26.53° (1 3)	19	3.24	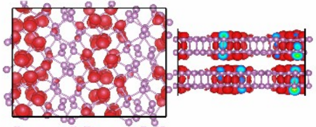	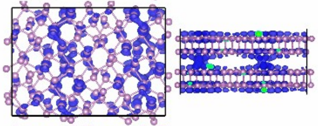
20.05° (1 4)	33	3.22	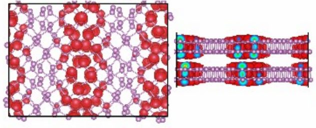	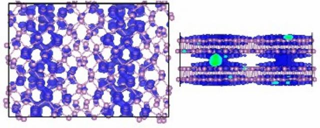
16.11° (1 5)	51	3.22	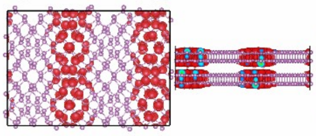	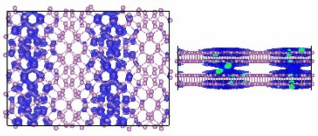

Figure S5. Charge densities of the CBM and VBM in bilayer BP with different twist angles. The superlattice is dependent on the values of p and q, which are listed in **Table S2**. Charge separation is determined by the values of twist angles rather than the superlattice. The VBM and CBM states are separated into different patterns as the twist angle lower to 38.94°.

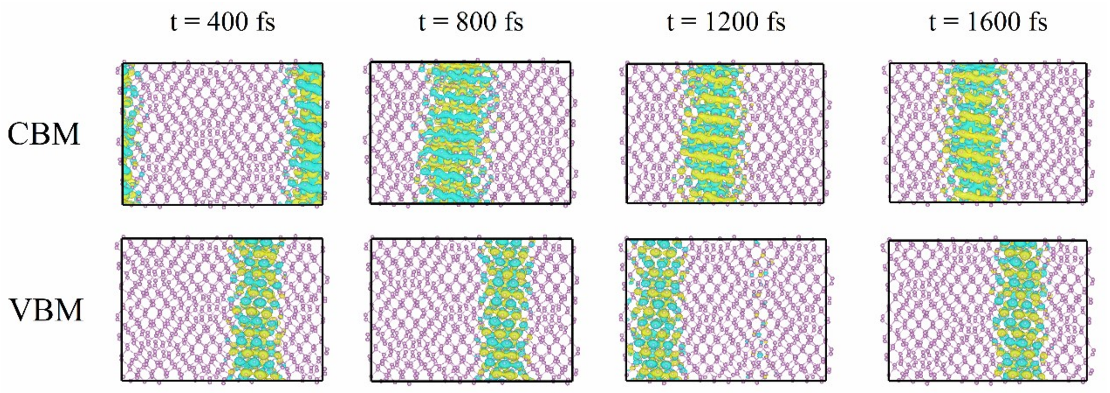

Figure S6. Charge densities for the CBM and VBM at 400, 800, 1200, and 1600 fs of the 11.54° twisted angle system at room temperature. Electron and hole separation holds during the MD simulation.

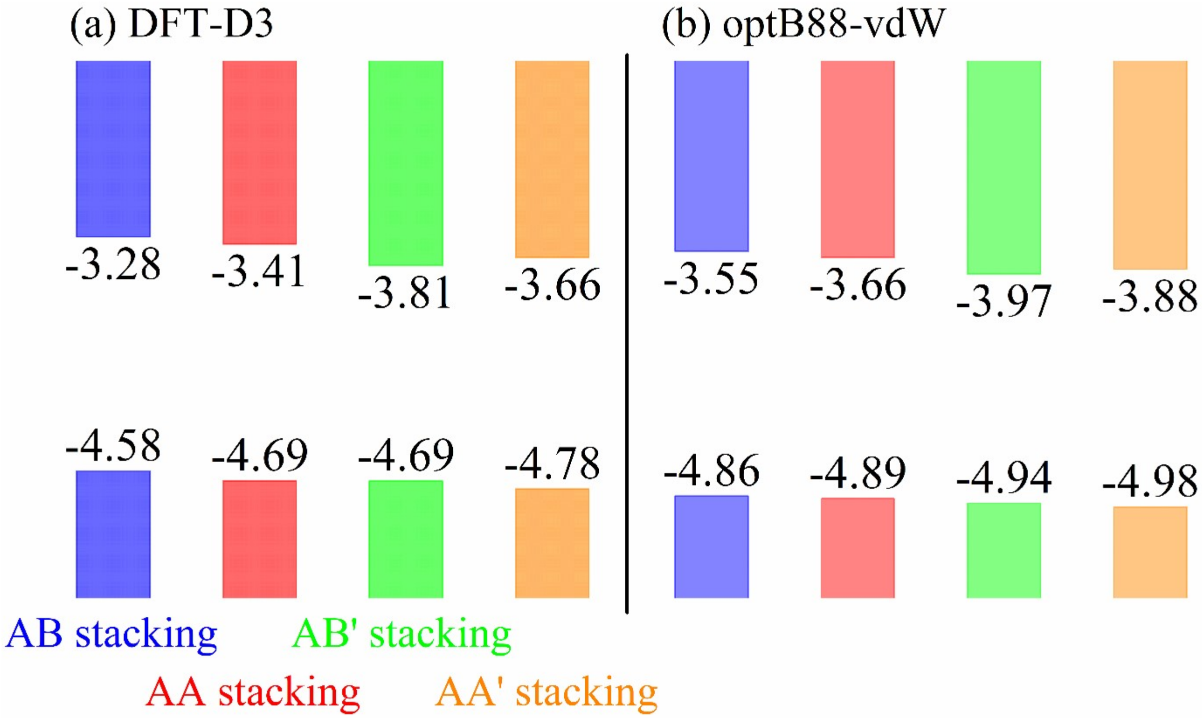

Figure S7. Potentials of VBM and CBM in high-symmetry stackings, including AA, AA’, AB, and AB’ staking configurations calculated by (a) DFT-D3[4] and (b) optB88-vdW.[5-6] The both methods show same orders.

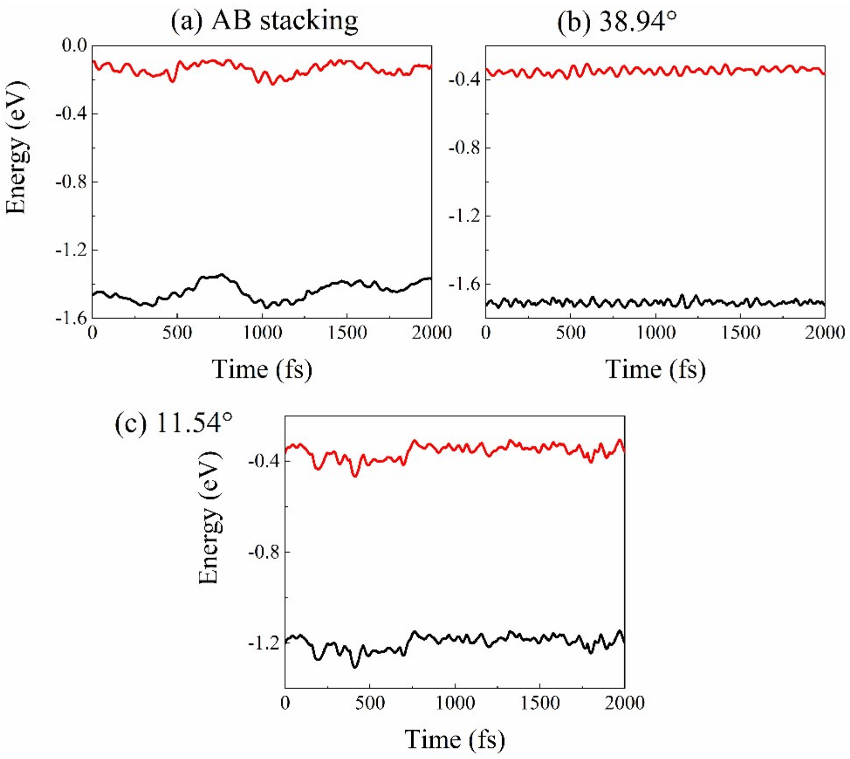

Figure S8. Time evolution orbital energy of the CBM and VBM for bilayer BP with (a) AB stacking, (b) 38.94°, and (c) 11.54° twist angles. The bandgap of AB stacking is scaled to the experimental value by scissor operator. The same constant was applied to the systems with 38.94° and 11.54° twist angles. The fluctuations decrease on the sequence: AB > 11.54° > 38.94°, rationalizing the decoherence times are opposite to this trend, **Fig. 4b** and **Table 2**.

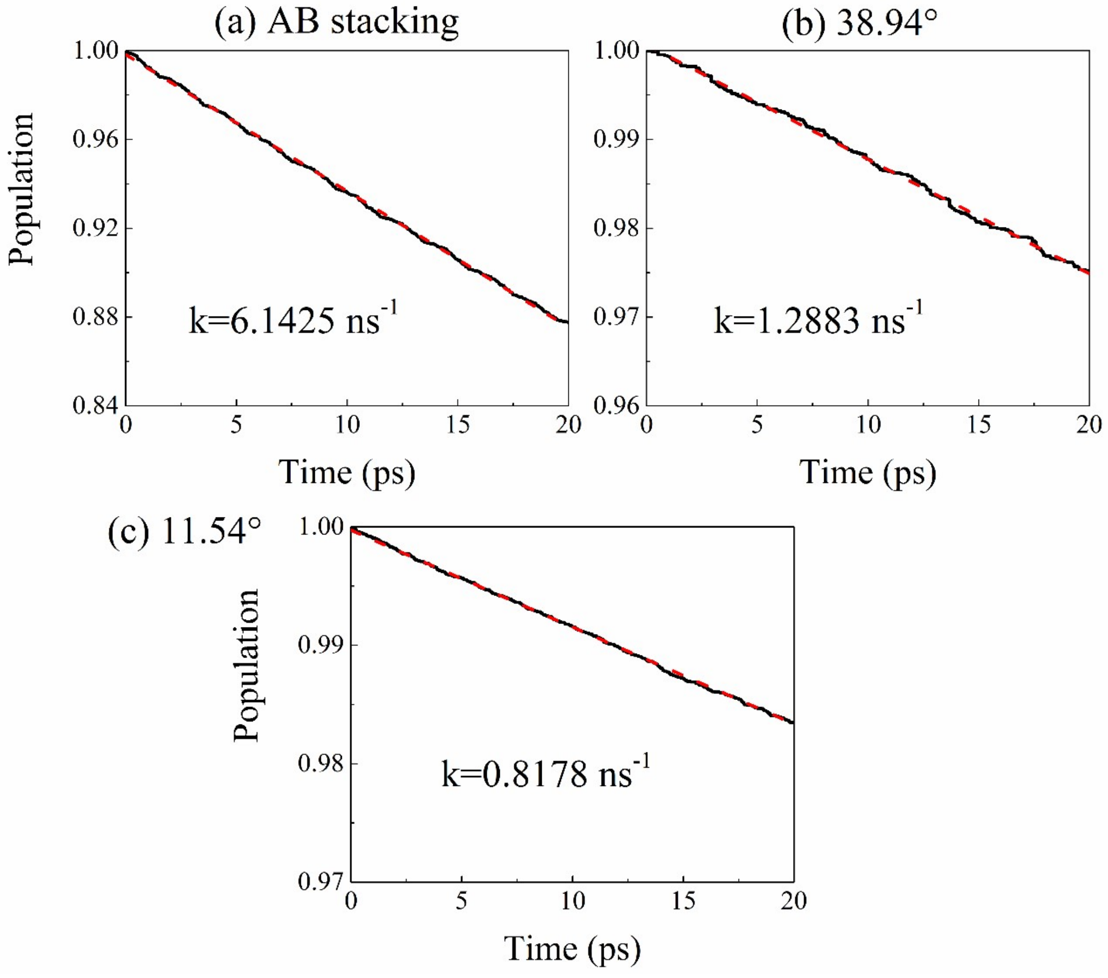

Figure S9. Time evolution population of the first excited–state (CBM) for bilayer BP with (a) AB stacking, (b) 38.94°, and (c)11.54° twist angles. The dashed red lines represent the fitted data of the short-linear decay to the exponential function, $P(t) = exp(- t/\tau) \approx 1 - t/\tau$.

Table S1. Bandgaps (eV), Interlayer Distance (Å), and Interaction Energy (eV) Calculated by using DFT-D3 and optB88-vdW Functionals for High-Symmetry Stackings of Bilayer BP. The Bandgaps Are Corrected by Scissors Operator.

Stackings	Methods	Interlayer Distance	Interaction Energy	Bandgap
AB	DFT-D3	3.10	0.31	1.30
	optB88-vdW	3.16	0.44	1.31
AB’	DFT-D3	3.30	0.24	0.88
	optB88-vdW	3.37	0.37	0.97
AA	DFT-D3	3.51	0.20	1.28
	optB88-vdW	3.49	0.36	1.23
AA’	DFT-D3	3.75	0.15	1.12
	optB88-vdW	3.72	0.29	1.10

Table S2. Bilayer BP with Different Twist Angles Calculated by Using VASP.

Sacking Model	(p q)	Superlattice	Interlayer Distance (Å)
70.53°	(1 1)	3	3.08
55.88°	(3 4)	41	3.15
50.47°	(2 3)	11	3.19
38.94°	(1 2)	9	3.22
26.53°	(1 3)	19	3.24
20.05°	(1 4)	33	3.22
16.11°	(1 5)	51	3.22

REFERENCES

(1) Kresse, G.; Furthmüller, J., Efficient iterative schemes for ab initio total-energy calculations using a plane-wave basis set. *Phys. Rev. B* **1996,** *54*, 11169-11186.

(2) Kühne, T. D.; Iannuzzi, M.; Del Ben, M.; Rybkin, V. V.; Seewald, P.; Stein, F.; Laino, T.; Khaliullin, R. Z.; Schütt, O.; Schiffmann, F., CP2K: An electronic structure and molecular dynamics software package-Quickstep: Efficient and accurate electronic structure calculations. *J. Chem. Phys.* **2020,** *152*, 194103.

(3) Perdew, J. P.; Burke, K.; Ernzerhof, M., Generalized Gradient Approximation Made Simple. *Phys. Rev. Lett.* **1996,** *77*, 3865-3868.

(4) Grimme, S.; Antony, J.; Ehrlich, S.; Krieg, H., A consistent and accurate ab initio parametrization of density functional dispersion correction (DFT-D) for the 94 elements H-Pu. *J. Chem. Phys.* **2010,** *132*, 154104.

(5) Klimeš, J.; Bowler, D. R.; Michaelides, A., Chemical accuracy for the van der Waals density functional. *J. Phys.: Condens. Matter* **2009,** *22*, 022201.

(6) Klimeš, J.; Bowler, D. R.; Michaelides, A., Van der Waals density functionals applied to solids. *Phys. Rev. B* **2011,** *83*, 195131.

(7) Blöchl, P. E., Projector augmented-wave method. *Phys. Rev. B* **1994,** *50*, 17953-17979.

(8) Wei, Y.; Fang, W.-H.; Long, R., Covalent Functionalized Black Phosphorus Greatly Inhibits Nonradiative Charge Recombination: A Time Domain Ab Initio Study. *J. Phys. Chem. Lett.* **2020,** *11*, 478-484.

(9) Wei, Y.; Long, R., Grain Boundaries Are Benign and Suppress Nonradiative Electron-Hole Recombination in Monolayer Black Phosphorus: A Time-Domain Ab Initio Study. *J. Phys. Chem. Lett.* **2018,** *9*, 3856-3862.

(10) Goedecker, S.; Teter, M.; Hutter, J., Separable dual-space Gaussian pseudopotentials. *Phys. Rev. B* **1996,** *54*, 1703-1710.

(11) VandeVondele, J.; Hutter, J., Gaussian basis sets for accurate calculations on molecular systems in gas and condensed phases. *J. Chem. Phys.* **2007,** *127*, 114105.

(12) Zapata, F. *nano-qmflows*, 0.8.2; github: 2020.

(13) Akimov, A. V.; Prezhdo, O. V., The PYXAID Program for Non-Adiabatic Molecular Dynamics in Condensed Matter Systems. *J. Chem. Theory Comput.* **2013,** *9*, 4959-4972.

(14) Akimov, A. V.; Prezhdo, O. V., Advanced Capabilities of the PYXAID Program: Integration Schemes, Decoherence Effects, Multiexcitonic States, and Field-Matter Interaction. *J. Chem. Theory Comput.* **2014,** *10*, 789-804.

(15) Kang, P.; Zhang, W.-T.; Michaud-Rioux, V.; Kong, X.-H.; Hu, C.; Yu, G.-H.; Guo, H., Moiré Impurities in Twisted Bilayer Black Phosphorus: Effects on the Carrier Mobility. *Phys. Rev. B* **2017,** *96*, 195406.

(16) Shu, H.; Li, Y.; Niu, X.; Wang, J., The stacking dependent electronic structure and optical properties of bilayer black phosphorus. *Phys. Chem. Chem. Phys.* **2016,** *18*, 6085-6091.

(17) Fang, T.; Liu, T.; Jiang, Z.; Yang, R.; Servati, P.; Xia, G., Fabrication and the Interlayer Coupling Effect of Twisted Stacked Black Phosphorus for Optical Applications. *ACS Appl. Nano Mater* **2019,** *2*, 3138-3145.

(18) Ji, Z.; Hong, H.; Zhang, J.; Zhang, Q.; Huang, W.; Cao, T.; Qiao, R.; Liu, C.; Liang, J.; Jin, C.; Jiao, L.; Shi, K.; Meng, S.; Liu, K., Robust Stacking-Independent Ultrafast Charge Transfer in MoS_2/WS_2 Bilayers. *ACS Nano* **2017,** *11*, 12020-12026.

(19) Wu, L.; Cong, C.; Shang, J.; Yang, W.; Chen, Y.; Zhou, J.; Ai, W.; Wang, Y.; Feng, S.; Zhang, H.; Liu, Z.; Yu, T., Raman scattering investigation of twisted WS_2/MoS_2 heterostructures: interlayer mechanical coupling versus charge transfer. *Nano Res.* **2021,** *14*, 2215-2223.

(20) Shulenburger, L.; Baczewski, A. D.; Zhu, Z.; Guan, J.; Tománek, D., The Nature of the Interlayer Interaction in Bulk and Few-Layer Phosphorus. *Nano Lett.* **2015,** *15*, 8170-8175.

(21) Hu, Z.-X.; Kong, X.; Qiao, J.; Normand, B.; Ji, W., Interlayer electronic hybridization leads to exceptional

thickness-dependent vibrational properties in few-layer black phosphorus. *Nanoscale* **2016,** *8*, 2740-2750.

(22) Bardeen, J.; Shockley, W., Deformation Potentials and Mobilities in Non-Polar Crystals. *Phys. Rev.* **1950,** *80*, 72-80.

(23) Qiao, J.; Kong, X.; Hu, Z.-X.; Yang, F.; Ji, W., High-mobility transport anisotropy and linear dichroism in few-layer black phosphorus. *Nat. Commun.* **2014,** *5*, 4475.

(24) He, Y.; Zhang, M.; Shi, J.-j.; Cen, Y.-l.; Wu, M., Improvement of Visible-Light Photocatalytic Efficiency in a Novel InSe/Zr_2CO_2 Heterostructure for Overall Water Splitting. *J. Phys. Chem. C* **2019,** *123*, 12781-12790.

(25) Cai, Y.; Zhang, G.; Zhang, Y.-W., Polarity-Reversed Robust Carrier Mobility in Monolayer MoS_2 Nanoribbons. *J. Am. Chem. Soc.* **2014,** *136*, 6269-6275.

(26) Zhu, Y.; Gong, L.; Zhang, D.; Wang, X.; Zhang, J.; Zhang, L.; Dai, L.; Xia, Z., Catalytic origin and universal descriptors of heteroatom-doped photocatalysts for solar fuel production. *Nano Energy* **2019,** *63*, 103819.

(27) Cheng, L.; Liu, Y., What Limits the Intrinsic Mobility of Electrons and Holes in Two Dimensional Metal Dichalcogenides? *J. Am. Chem. Soc.* **2018,** *140*, 17895-17900.

(28) Zhu, Y.; Long, R., Density Functional Theory Half-Electron Self-Energy Correction for Fast and Accurate Nonadiabatic Molecular Dynamics. *J. Phys. Chem. Lett.* **2021,** *12*, 10886-10892.